JOURNAL OF AIRCRAFT
Vol. 43, No. 3, May–June 2006

Embedded Laser Doppler Velocimetry Boundary-Layer Investigation on a Tilt-Rotor Blade

C. Barla,* E. Berton,† D. Favier,‡ and C. Maresca§
Centre National de la Recherche Scientifique and Université de la Méditerranée, 13288 Marseille Cedex 09, France

A fundamental study is made of a rotating boundary layer (BL) in the inboard region of a tilt-rotor blade, using an embedded laser Doppler velocimetry probe inside a rotating blade. Velocity measurements have been performed to get insight into the BL behavior around a blade section close to the rotor hub. BL transition and separation phenomena are investigated on the basis of both chordwise and spanwise velocity profiles measured for different collective pitch angles on a two-bladed hovering rotor. The velocity experimental data bank appears to be in good agreement with theoretical velocity profiles in attached flow conditions (laminar, transitional, or turbulent). Moreover, validation of a transitional criterion based on the second thickness of energy δ_3' of the BL is extended to the rotational flow configuration. Usually such a configuration classically exhibits a separation of the BL for high collective pitch angles. However, in the particular case of a high twisted tilt-rotor blade operating in hover, centrifugal effects are shown to be responsible for an important delay in the BL separation process.

Nomenclature

c	=	blade chord, m
l	=	blade length, m
R	=	rotor radius, m
Re_c	=	Reynolds number, $c \cdot V_\infty/\nu$
r	=	radial abscissa on the rotor blade, m
U_{42}, U_{37}	=	measured velocity components, $\mathrm{m} \cdot \mathrm{s}^{-1}$
V_t, V_r	=	reconstructed tangential and radial velocity components, $\mathrm{m} \cdot \mathrm{s}^{-1}$
V_∞	=	freestream velocity, $\Omega \cdot r$, $\mathrm{m} \cdot \mathrm{s}^{-1}$
x, y, z	=	chordwise, spanwise, and normal to the wall unit vector
$\alpha_{r/R=0.3}$	=	blade angle of attack at $r/R = 0.3$, deg
δ_3'	=	second thickness of energy of the boundary layer, $\int_0^\delta \frac{V_t^2}{V_\infty^2} \cdot \left(1 - \frac{V_t}{V_\infty}\right) \mathrm{d}z$
η	=	reduced altitude of Blasius, $z \cdot (V_\infty/\nu \cdot z)^{1/2}$
$\theta_{r/R=0.3}$	=	blade collective pitch angle at $r/R = 0.3$, deg
ν	=	air cinematic viscosity, $\mathrm{m}^2 \cdot \mathrm{s}^{-1}$
Ω	=	rotational frequency, $\mathrm{rad} \cdot \mathrm{s}^{-1}$

Introduction

TILT-ROTOR blade aerodynamics appears to be different when compared to conventional helicopter blades. Indeed, tilt-rotor blades are generally characterized by high levels of twist, by solidity, and by a complex distribution of the blade loads. Many studies on tilt-rotors have been performed to improve and validate the aerodynamics prediction of numerical models. Such models have often been directly derived from helicopters rotor blade studies. A lot of numerical studies aim at better modeling the distortion and the evolution of the wake in different flight configurations. However, there are very few experimental databases dedicated and well adapted to a proper validation of such numerical approaches. The complex nature of the tilt-rotor wake resulting from interactions with other aircraft components (wing, fuselage, etc.) explains why few experimental studies are available. Experimental studies of tilt-rotors have been performed by NASA with the tilt-rotor aeroacoustic model (TRAM)[1] in the Druits–Netherlands Wind Tunnel and measurements have mainly been with reference to overall performances and blade airloads.[2] This experimental program consisted in a series of aeroacoustic tests designed to validate numerical outputs, that is, aerodynamic, acoustic, and performance prediction analyses.[3] For the same rotor geometry, Johnson has also developed the CAMRAD II simulation code, with the intent to model the evolution of the tilt-rotor wake.[4,5] Such a code takes into account the boundary-layer (BL) behavior on the blade surface and more specifically the occurrence of the BL separation delay that is is due to rotational effects.[6] Although CAMRAD II provided good results in hovering and transition flight configurations, cruise flight needs more validation efforts. Moreover, in a descent flight condition, the tilt-rotor is also characterized by strong rotor–wake interactions. This blade–vortex interaction (BVI) causes significant changes in unsteady blade loads and generates high vibrations and impulsive noise.[7] Recently, wind-tunnel measurements and flight tests have shown that BVI remains the dominant noise source for a wide range of operating conditions.[8,9] Validation of aeroacoustic analyses requires more detailed and accurate wake measurements. These requirements include the three-dimensional distorted wake geometry and pertinent data on tip vortices (core size and strength evolution along their paths).[10] To our knowledge, most studies on highly twisted tilt-rotor blades in rotation present global results with no BL measurements. Moreover, other studies have been aimed at better understanding and modeling the interaction effects between the rotor wake and a fixed wing.[11]

Most of validation and improvement of numerical works on BL characteristics have been undertaken only for helicopter rotor blade types without centrifugal effects. In particular, the flow physical phenomena occurring in the region very close to the tilt-rotor blades, such as BL transition, separation, and dynamic stall, require more local and detailed data. One of the conditions for dynamic stall onset is the formation of a single vortex near the leading-edge region. In this region, the flow separation generates a shear layer that quickly rolls up into a strong vortex. The process of dynamic stall was the source of large amounts of research in the past two decades.[12,13] Three

Received 7 February 2005; revision received 6 June 2005; accepted for publication 10 June 2005.

*Ph.D. Student, Laboratory of Aerodynamics and Biomechanics of Motion, Unité de Service et de Recherche, LABM-USR 2164; barla@labm.univ-mrs.fr.

†Research Scientist, Laboratory of Aerodynamics and Biomechanics of Motion, Unité de Service et de Recherche, LABM-USR 2164; currently Professor, Université de la Méditerranée, Movement and Perception Laboratory, LMP-UMR 6152; eric.berton@univmed.fr. Member AIAA.

‡Senior Research Scientist, Laboratory of Aerodynamics and Biomechanics of Motion, Unité de Service et de Recherche, LABM-USR 2164; favier@labm.univ-mrs.fr. Senior Member AIAA.

§Senior Research Scientist, Laboratory of Aerodynamics and Biomechanics of Motion, 2164; maresca@labm.univ_mrs.fr. Associate Fellow AIAA.

main mechanisms can cause the dynamic stall onset: the bursting of a laminar separation bubble, adverse pressure gradients, or a shock. Carr et al.[14] established that the onset of dynamic stall can be due to the bursting of the laminar separation bubble that is forming while the airfoil is pitching upstroke. Other authors have provided experimental data concerning the particular phenomenon that leads to the BL change of state around oscillating airfoil in two- and three-dimensional flow configurations.[15,16] For steady flow conditions, the intermittent nature of the flow separation near stall has been observed, which is shown to be linked to the Strouhal number and to the structure and the location of the separation bubble.[17] More recently, Rinoie and Takemura have also measured the evolution of short and long bubbles that are developing on the upper side of a NACA0012 airfoil near stall conditions by means of laser light sheet visualization and surface pressure distributions.[18] Numerical simulations of the flow evolution giving raise to a laminar BL followed by a turbulent reattachment remains difficult to predict accurately for Reynolds-average Navier–Stokes, large-eddy simulation, or direct numerical simulation, methods because of the complex nature of the transition process.[19,20] Indeed, mean and fluctuating velocities are very sensitive to the modeling of the transition zone according to the local mesh refinement and turbulence models used. Moreover, computational fluid dynamics methods have almost simulated two-dimensional flow configurations but failed to capture the detailed flow features of three-dimensional bubbles.

Within this scope, the present study aims to investigate the BL on a tilt-rotor blade by means of embedded laser Doppler velocimetry (ELDV) measurements and is more specifically focused on the BL separation delay due to the rotation in hovering flight conditions. The following sections will, first, give a short description of the experimental setup and the associated measurements methods. The paper will then successively present the tilt-rotor blade geometry and the hovering parametric conditions. A detailed description of the ELDV characteristics and its embedment is given, as well as the velocity components (chordwise V_t and spanwise V_r) determination procedure. The BL behavior is deduced from velocity profiles measured at three pitch angle values: two below the static stall angle, that is, $\theta_{r/R=0.3} = 10.22$ deg and 15.38 deg and one above the static stall angle, that is, $\theta_{r/R=0.3} = 24.75$ deg. Particular attention is paid to the flow generated at the highest collective pitch angle value giving raise to the BL separation delay.These results are also compared to theoretical velocity profiles (Pohlhausen and $1/n$ law) to provide validation of a transition criteria based on the second thickness of energy δ_3' of the BL.

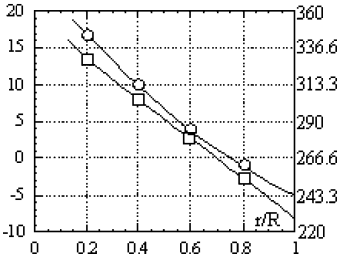

Fig. 1 Twist and chord distributions along blade span: ○, twist (degrees) and □, chord (millimeters).

Experimental Methodology

Rotor Blade Geometry

The rotor blade geometry is similar to the CAMRAD II model of TRAM.[21] The linear part of the twist, relative to the blade sections located in the region close to the rotor hub, allows the implementation of the ELDV optical head and a 45-deg mirror inside the blade, where converging laser beams emerge to create the measurement volume. At three chordwise stations, $x/c = 0.10$, 0.33, and 0.54, located at the blade section $r/R = 0.3$, the tangential and radial velocity components have been measured in the BL flow region from $0.3 \leq z \leq 20$ mm along the normal distance to the wall (corresponding to $1 < \eta < 80$).

The rotor is two bladed, $b = 2$, with a radius $R = 1.5$ m, a blade length $l = 1.26$ m, and a solidity $\sigma = 0.1$. Twist and chord distributions of the blade are shown in Fig. 1. The twist law is given according to the convention of twist = 0 deg at $r/R = 0.75$. Three different NACA series airfoils are distributed all along the blade span (NACA64528, 64118, and 64152) as shown in Fig. 2.

The rotor hub is mounted on a supporting mast, and the rotation center is located 2.9 m above the ground. The model rotor is composed of a fully articulated hub that can be equipped with an interchangeable set of blades. The scaled rotor is set up on the hovering test rig of the Laboratory of Aerodynamics and Biomechanics of Motion (LABM) and is running in hover with an induced flow blowing from the bottom to the top to avoid ground and recirculation effects.

Measurement Method

The instrumented rotor blades have been designed according to requirements prescribed by centrifugal forces, masses of the embedded components, and readability of beams alignment. The laser beams issued from the laser source are conducted to the blade through fixed optical fibers, a light transmitter, and rotating optical fibers, which are connected to the rotating blade by the guiding tube (Fig. 3).

The transmitter allows the passing of the signal light from a fixed reference frame of the laboratory (white area in Fig. 3) to the rotating frame of the blade (gray part in Fig. 3). The rotating transmitter

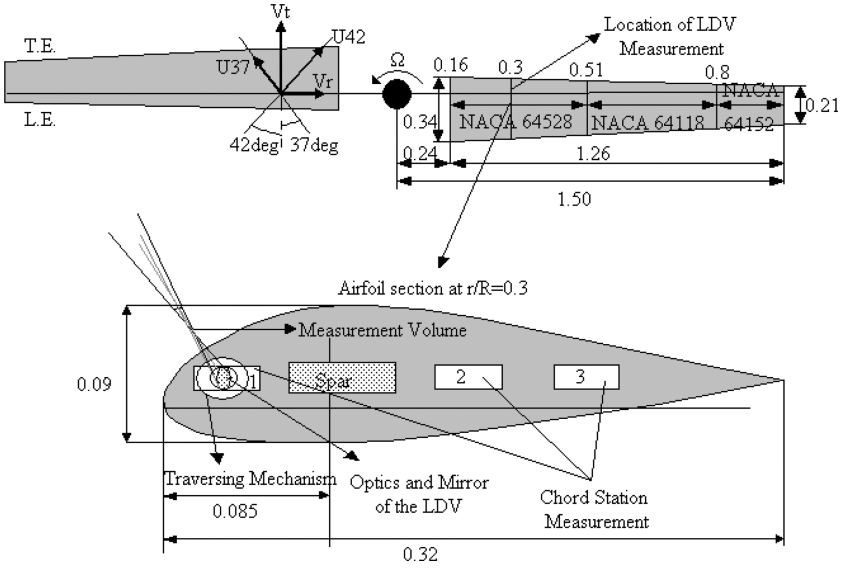

Fig. 2 Rotor geometry and airfoil section characteristics, $\sigma = 0.1$ and $n_{max} = 1300$ rpm.

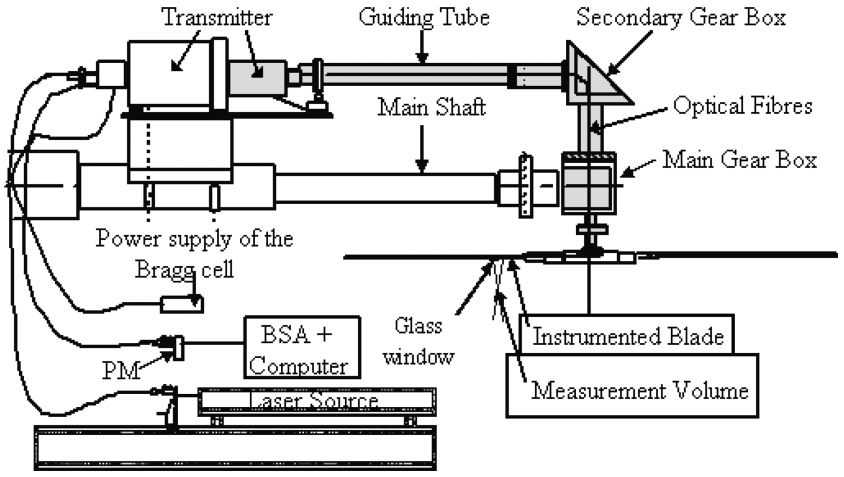

Fig. 3 Components of ELDV method.

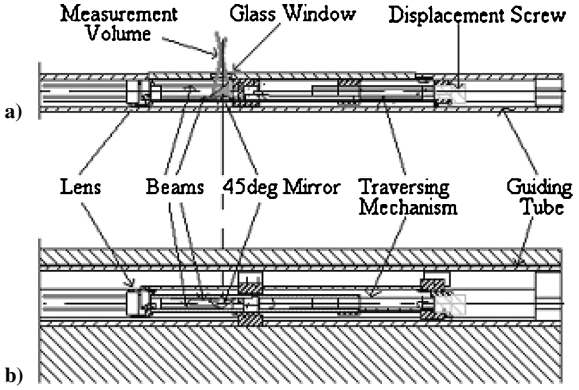

Fig. 4 Instrumented blade: a) side view and b) top view.

is the most critical part of the ELDV system.[22] First, it transmits the input laser beam on axis during rotation while maintaining a constant linear polarization. Second, it transmits the received light in a coaxial mode to an external multimode fiber link. When particles are seeded in the flow and pass through the measurement volume, the backscattered signals are collected through receiving optical fibers to the fixed components of the velocimeter system (photomultipliers, burst spectrum analyzer, computer, etc.). The seeding of the flow is achieved by emitting particles of an oil mixture ($\Phi \approx 1\ \mu$m diameter) seeded in the entire volume of the servicing hall, where the hovering rotor is settled. As shown in Fig. 2, one of the blades is equipped with the ELDV system, and an adjustable mass is mounted in the other to balance accurately the weight distribution of the first blade. The probe can be set at different positions to survey three chordwise stations 1, 2, and 3 in Fig. 2.

The main components of this particular ELDV system are directly embedded in the rotating instrumented blade (Fig. 4). Two parallel beams, coming from the optical fibers, arrive through the probe to the lens, converge to the mirror, and focus through the optical window (mounted flush to the blade surface) in the measurement volume (Figs. 2 and 4). The measurement volume can be displaced normally to the blade surface by means of a translation screw, which changes the relative position between the lens and the mirror. The farther the lens is from the mirror, the closer the measurement volume to the blade surface is.

Table 1 lists the main characteristics of the present ELDV system and the corresponding dimensions of the measurement volume. The dz length allows a measurement to the wall as close as 0.3 mm, and the focal lens provides an exploration along the normal to the wall of 20 mm.

Measurement of V_t and V_r Velocity Components

As shown in Fig. 2, the two measured velocities U_{42} and U_{37} allow the reconstruction of the tangential V_t and radial V_r velocity components. For each x/c chord location, the probe can be mounted in two different fixed positions obtained by rotating the probe around its axis. By construction and in the first position, the angle between the measured velocity U_{42} and the chord direction is equal to 42 deg, whereas in the second position, the angle between the measured velocity and the chord direction is 37 deg. According to Fig. 2, the radial and chordwise velocity components are given by

$$V_t = U_{42} \cdot \cos(42\ \text{deg}) - U_{37} \cdot \cos(37\ \text{deg})$$

$$V_r = -U_{42} \cdot \sin(42\ \text{deg}) - U_{37} \cdot \sin(37\ \text{deg}) \qquad (1)$$

The two velocities components U_{42} and U_{37} are measured for three chordwise stations, $x/c = 0.10$, 0.33, and 0.54, at three different collective pitch angles, $\theta_{r/R=0.3} = 10.22$, 15.38, and 24.75 deg.

Table 1 Laser velocimeter specifications

Optical head	Specification	Units
Velocity component	U_{42} or U_{37}	m/s
Focal lens	50	mm
Laser source wave length	514,5	nm
Measurement volume		
dx	0.041	mm
dz	0.510	mm
Fringe spacing	0.0032	mm
Number of fringes	13	
Axial working length	46	mm

Data Acquisition

Backscattered signals from the measurement volume are analyzed through a burst spectrum analyzer. As shown in Fig. 5a, a classical acquisition corresponds to 4000 samples of U_{42} or U_{37} velocity components, accumulated on a single rotation cycle and statistically reduced (rms value, histogram, mean value, etc.). Figure 5b presents an example of the histogram relative to the U_{42} velocity component, whereas Fig. 5c shows the variation of U_{42} and U_{37} measured velocities as a function of the normal distance to the blade surface. Velocity components V_t and V_r are then obtained from Eq. (1).

Experimental Uncertainty

As in a classical laser Doppler anemometry technique, there are random errors due to the statistical nature of the ELDV measurements and systematic errors due to pressure gradient of the flow. These two kinds of errors are estimated next for each velocity component U_{42} and U_{37} (Ref. 22). Random errors can be decomposed in three parts. The first is due to the use of the Doppler signals frequencies acquisition system, ε_{11}; the second comes from the unpunctual and statistical nature of the measurements based on seeding particles that are transiting within the measurement volume, ε_{12}; finally,

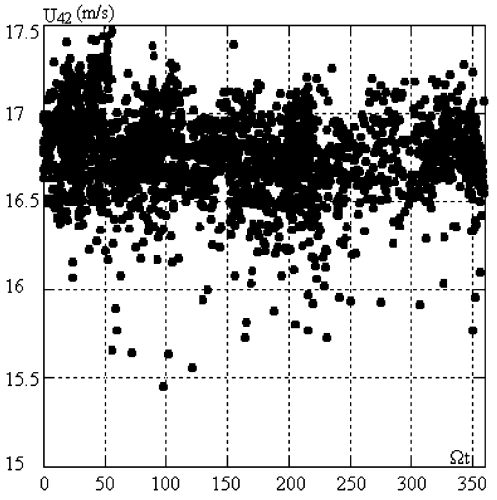

a) U_{42} velocity component over single period of rotation

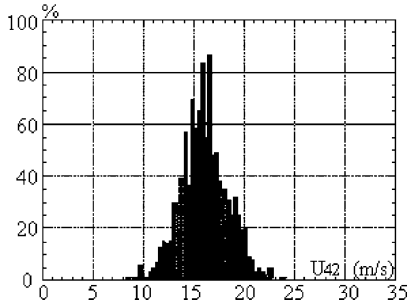

b) Histogram obtained on U_{42} component

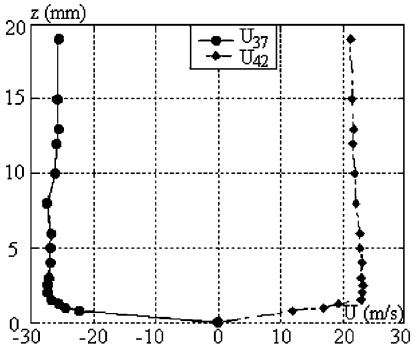

c) Evolution of velocity components

Fig. 5 Velocity data acquisition example at $\theta_{r/R=0.3} = 15.38$ deg and $x/c = 0.33$.

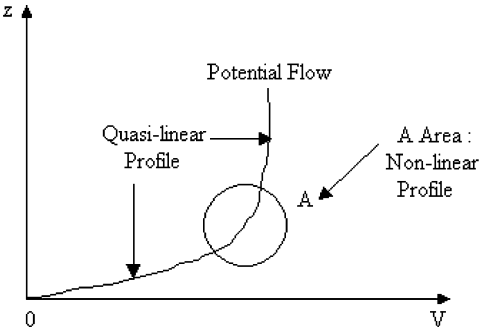

Fig. 6 Area favorable to systematic error.

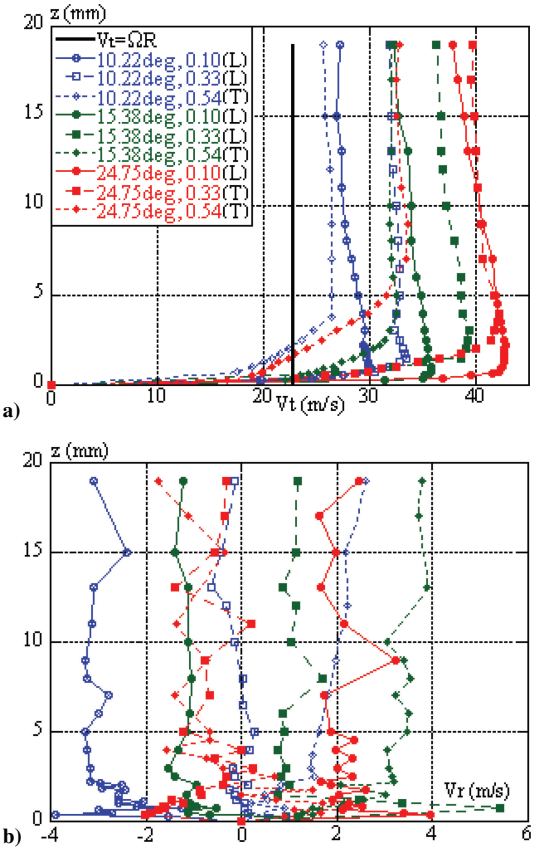

Fig. 7 Evolution of velocities as a function of z for three $\theta_{r/R=0.3}$ values and three chordwise positions: a) V_t and b) V_r.

the last ones come from other random parameters, such as the reliability of optoelectronics components, ε_{13}. The systematic error is the result of the measurement point allocation to the midpoint of the measurement volume. Such a systematic error would not exist if the velocity profile $V = V(z)$ were linear. However, there is an area within the BL thickness where $V(z)$ is strongly nonlinear (Fig. 6). Quantification of this kind of error has been achieved in a previous study[22] at LABM and has been deduced from comparisons between laminar (and turbulent) measured velocity profiles and theoretical profiles that have been statistically treated. Usually, measurements data close to the wall show that the systematic error remains less than 1% for each velocity component performed: $(\varepsilon_2)_{42} < 1\%$ and $(\varepsilon_2)_{37} < 1\%$. When all of the preceding measurement errors are added, the total error is estimated for each velocity component as shown in Table 2.

During the present tests, controls have been performed for the maximum measurement error of the U_{42} velocity component, which is less than 2.4%, and of the U_{37} component, which is less than 3%.

Results and Discussion

A first set of experiments have been conducted at a relatively low rotational speed, $\Omega = 480$ rpm (50 rad.s-1), to adjust the embedded velocimeter acquisition procedure. The chordwise and spanwise velocity profiles V_t and V_r have been measured at $r/R = 0.3$ (NACA64528 airfoil section) at three chordwise stations, $x/c = 0.10$, 0.33, and 0.54, and three collective pitch angle values, $\theta_{r/R=0.3} = 10.22$, 15.38, and 24.75 deg. The complete data set for chordwise V_t and spanwise V_r velocities has been gathered in Fig. 7 vs the normal distance to the wall z. Either a laminar (L) or turbulent (T) BL is denoted in Fig. 7. However, the data analysis and, particularly, the aerodynamic behavior around the blade airfoil section indicated by the BL velocity profiles requires the knowledge of the local angle of attack $\alpha_{r/R=0.3}$ as deduced from the collective pitch angle $\theta_{r/R=0.3}$, the local twist, and the flow-induced incidence α_i. The induced incidence α_i has been obtained from direct LDV measurements of the induced velocity field through the rotor disk. For a collective pitch angle $\theta_{r/R=0.3} = 10.22$ deg (respectively, 15.38 and 24.75 deg), the corresponding angle of attack $\alpha_{r/R=0.3}$ is equal to 7.2 deg (respectively, 10.3 and 19.1 deg).

Table 2 Total error of U_{42} and U_{37}

	Outside BL, %		Inside BL, %	
Error type	U_{42}	U_{37}	U_{42}	U_{37}
Random ε_{11}	$(\varepsilon_{11})_{42} < 1.3$	$(\varepsilon_{11})_{37} < 0.2$	$(\varepsilon_{11})_{42} < 1.0$	$(\varepsilon_{11})_{37} < 0.3$
Random ε_{12}	$(\varepsilon_{12})_{42} < 0.1$	$(\varepsilon_{12})_{37} < 0.6$	$(\varepsilon_{12})_{42} < 0.6$	$(\varepsilon_{12})_{37} < 1.5$
Random ε_{13}	——	——	$(\varepsilon_{13})_{42} < 0.2$	$(\varepsilon_{13})_{37} < 0.2$
Random ε_1 $(\varepsilon_{11} + \varepsilon_{12} + \varepsilon_{13})$	$(\varepsilon_1)_{42} < 1.4$	$(\varepsilon_1)_{37} < 0.8$	$(\varepsilon_1)_{42} < 1.8$	$(\varepsilon_1)_{37} < 2.0$
Systematic ε_2	$(\varepsilon_2)_{42} < 1.0$	$(\varepsilon_2)_{37} < 1.0$	$(\varepsilon_2)_{37} < 1.0$	$(\varepsilon_2)_{37} < 1.0$
Total ε $(\varepsilon_1 + \varepsilon_2)$	$\varepsilon_{42} < 2.4$	$\varepsilon_{37} < 1.8$	$\varepsilon_{42} < 2.8$	$\varepsilon_{37} < 3.0$

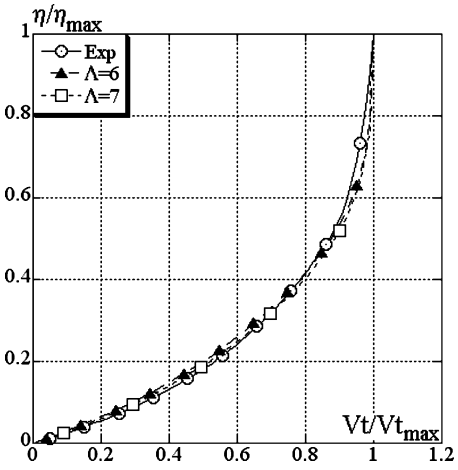

a) $\theta_{r/R=0.3} = 10.22$ deg, $x/c = 0.10$

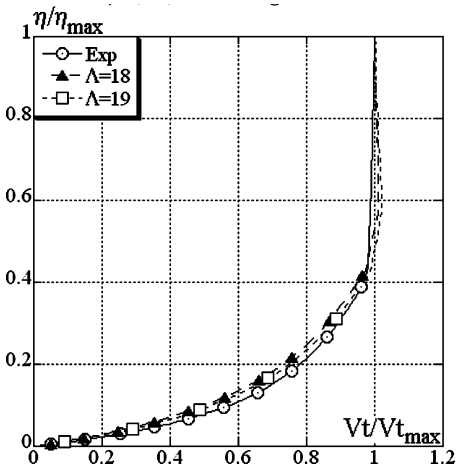

c) $\theta_{r/R=0.3} = 15.38$ deg, $x/c = 0.10$

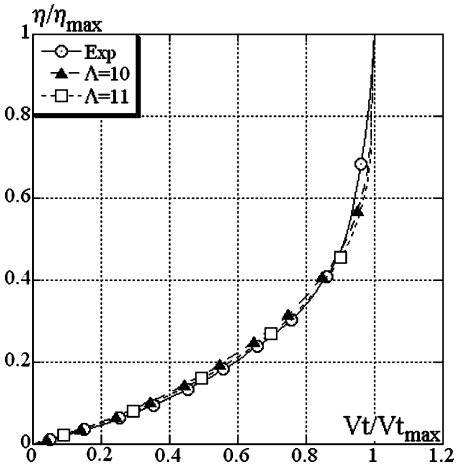

b) $\theta_{r/R=0.3} = 10.22$ deg, $x/c = 0.33$

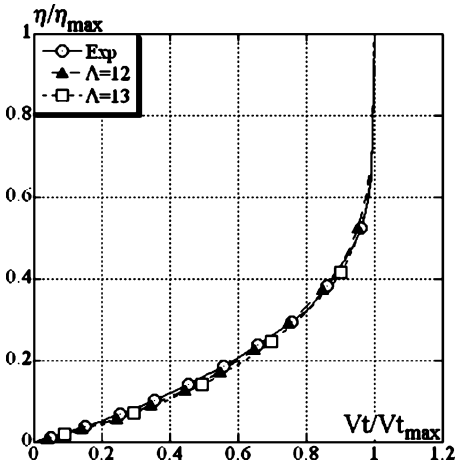

d) $\theta_{r/R=0.3} = 15.38$ deg, $x/c = 0.33$

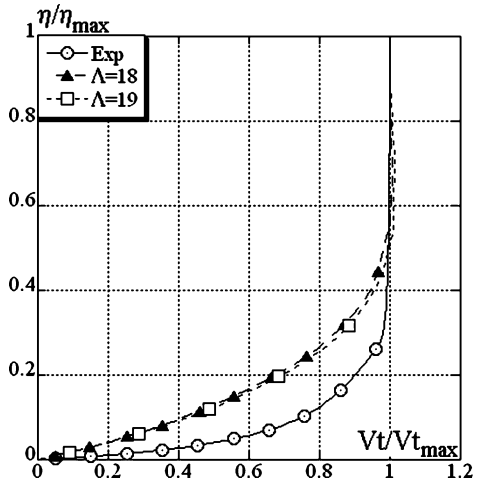

e) $\theta_{r/R=0.3} = 24.75$ deg, $x/c = 0.10$

Fig. 8 Comparisons of V_t tangential velocity with laminar velocity profile of Pohlhausen.

V_t Component Behavior

Figure 7a shows that the $V_t = V_t(z)$ evolution level increases with the collective pitch angle in the potential flow for each chord station. Moreover, the BL flow appears fully attached for all of the concerned x/c and $\theta_{r/R=0.3}$ parameters. Such a result, expected in the case of low collective pitch angles, is unexpected at $\theta_{r/R=0.3} = 24.75$ deg, which corresponds to a local angle of attack $\alpha_{r/R=0.3} = 19.1$ deg (corresponding to an aerodynamic incidence where the BL should be separated in steady uniform flow conditions). In addition, the V_t evolutions in Fig. 7a show an increase of the BL thickness when $\theta_{r/R=0.3}$ is increasing. For all of the $\theta_{r/R=0.3}$ values selected, the V_t evolutions in Fig. 7a exhibit an increase of the BL thickness when x/c increases along the chord. Moreover, the tangential velocity component outside the BL also increases between $x/c = 0.10$ and $x/c = 0.33$. This reveals a high-pressure gradient near the airfoil leading edge (due to significant airfoil curvature in this area). At the midchord station, $x/c = 0.54$, the measured tangential velocity V_t indicates a strong level decrease outside the BL region, which is linked with an important BL thickness. The spanwise velocity component evolution will be discussed to explain this strong decrease of V_t at the midchordwise station. Moreover, the more x/c and collective pitch angles are important, the thicker the BL is. As shown in Fig. 7a, the thickness of the BL increases from $\theta_{r/R=0.3} = 10.22$ deg and $x/c = 0.10$ up to $\theta_{r/R=0.3} = 24.75$ deg and $x/c = 0.54$. For this last value, the V_t profile exhibits a separation trend. However, for this unusual high collective pitch-angle value, the V_t profile clearly indicates that the BL is not separated and, thus, confirms the occurrence of a delay on the BL separation, which has been already observed in previous studies.[6] To characterize the nature of the BL, the measured V_t component has been compared to theoretical BL velocity profiles (Figs. 8 and 9) that correspond to either 1) a fourth polynomial order of Pohlhausen, which corresponds to a laminar BL with pressure gradient, where

$$V_t/V_{t\max} = 2 \cdot \eta - 2 \cdot \eta^3 + \eta^4 + (\Lambda/6) \cdot \eta \cdot (1-\eta)^3 \qquad (2)$$

where Λ is characteristic of the pressure gradient intensity or 2) a turbulent profile with a $1/n$ law evolution, where

$$V_t/V_{t\max} = (z/\delta)^{1/n} \qquad (3)$$

Figure 8 shows a comparison of the experimental V_t component evolution with Pohlhausen profiles for specific $(\theta_{r/R=0.3}, x/c)$ parameters giving a laminar BL.

Table 3 gives the evolution of the pressure gradient parameter Λ for the parametric conditions of this study. Such a parameter relative to the Pohlhausen law characterizes the laminar evolution of the BL. It clearly appears (Table 3, Figs. 9a–9d) that to match

Table 3 Value of pressure gradient Λ for laminar BL

$\theta_{r/R=0.3}$, deg	x/c	Λ
10.22	0.10	6
10.22	0.33	11
15.38	0.10	18
15.38	0.33	12
24.75	0.10	18

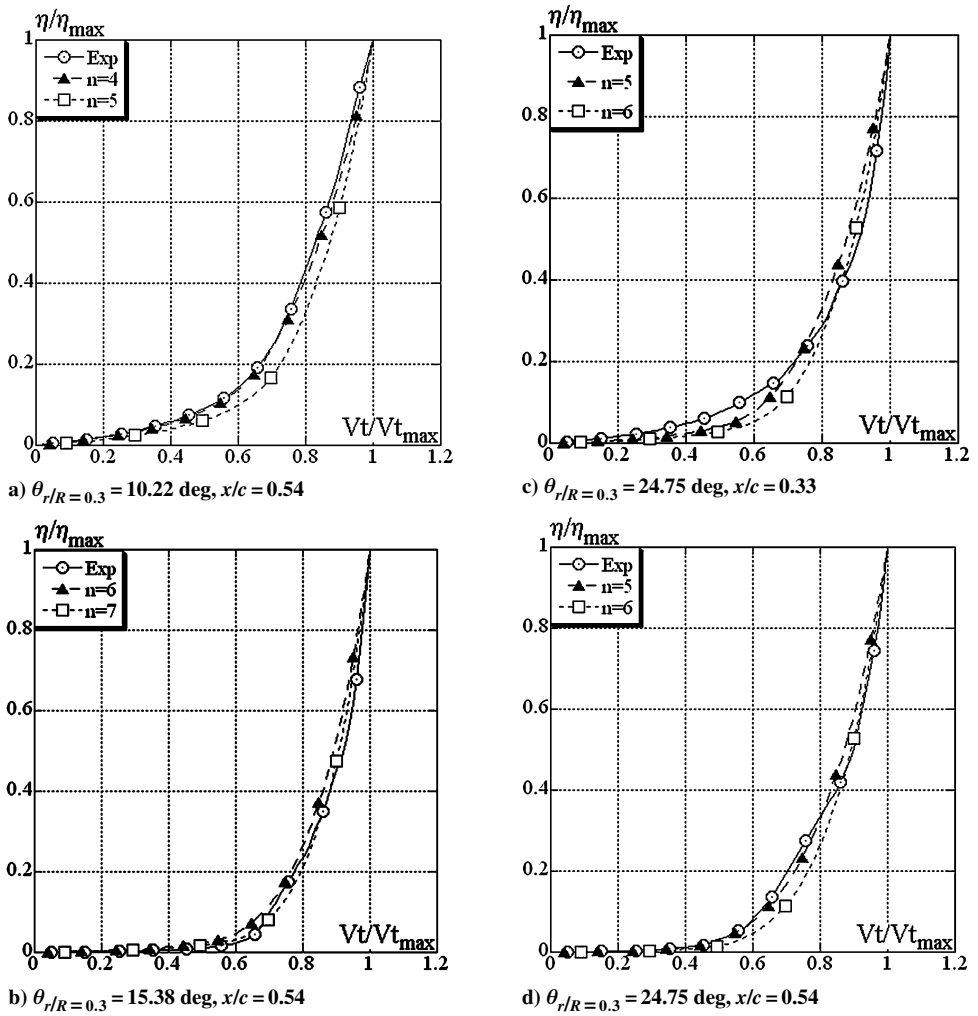

a) $\theta_{r/R=0.3} = 10.22$ deg, $x/c = 0.54$

c) $\theta_{r/R=0.3} = 24.75$ deg, $x/c = 0.33$

b) $\theta_{r/R=0.3} = 15.38$ deg, $x/c = 0.54$

d) $\theta_{r/R=0.3} = 24.75$ deg, $x/c = 0.54$

Fig. 9 Comparisons of V_t component with $1/n$ turbulent velocity profile.

Table 4 Centrifugal/centripetal flow directions

	θ, deg		
x/c	10.22	15.38	24.75
0.10	Centrifugal ≈ -3 m · s^{-1}	Centrifugal ≈ -1 m · s^{-1}	Centripetal ≈ 2 m · s^{-1}
	⬍	⬍	⬍
0.33	≈ 0 m · s^{-1}	Centripetal ≈ 1 m · s^{-1}	Centrifugal ≈ -1 m · s^{-1}
0.54	Centripetal ≈ 2 m · s^{-1}	Centripetal ≈ 3.5 m · s^{-1}	Centrifugal ≈ -1 m · s^{-1}

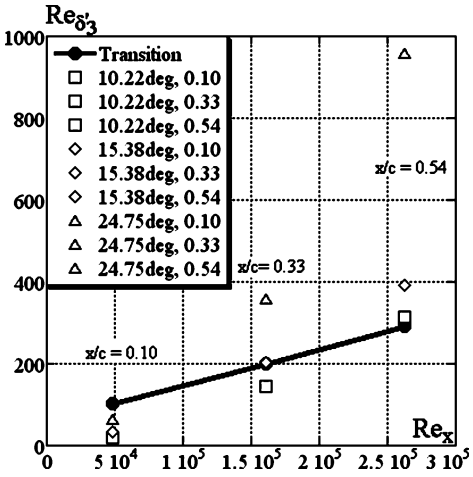

Fig. 10 Transition criterionbased on δ'_3.

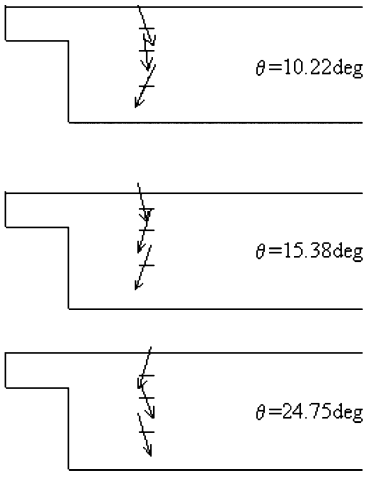

Fig. 11 Flow directions.

experimental velocity evolution well, Λ has to follow the increase of the collective pitch angle $\theta_{r/R=0.3}$. The velocity evolutions in Figs. 9a–9c are clearly representative of a BL laminar state. In these cases, the theoretical velocity profiles given by the Pohlhausen polynomial laws match the experimental velocity profiles well. In Fig. 9c, high values of Λ ($\Lambda = 18$ and 19) are required to well represent a laminar evolution. These Λ values reveal a very high negative pressure gradient when compared with classical BL evolutions around oscillating airfoil $-12 < \Lambda < 12$. Figure 9e ($x/c = 0.10$ and $\theta_{r/R=0.3} = 24.75$ deg) shows the limit of the Pohlhausen theoretical representation. Indeed, in this particular case of high collective pitch angle ($\theta_{r/R=0.3} = 24.75$ deg), the Pohlhausen law is not suitable to characterize the laminar behavior and centrifugal effects are shown to increase dramatically the negative pressure gradient at the leading edge while reducing the BL thickness (Fig. 9e). Comparisons shown in Figs. 9c and 9d ($x/c = 0.10$ and $x/c = 0.33$ and $\theta_{r/R=0.3} = 15.38$ deg) reveal a decrease of the Λ parameter from 18 to 12, respectively, which indicates that the negative pressure gradient becomes less important when x/c is increasing and a trend to separation on the V_t component near the leading edge.

For $x/c = 0.33$, $\theta_{r/R=0.3} = 24.75$ deg and $x/c = 0.54$, $10.22 \leq \theta_{r/R=0.3} \leq 24.75$ deg, Fig. 9 shows the turbulent evolution of the tangential velocity profile $V_t/V_{t\max}$. For such parametric conditions, the experimental $V_t/V_{t\max}$ evolutions are well fit by $1/n$ law turbulent profiles with an n value ranging from 5 to 7. The major result of this data set is, thus, the non-BL flow separation observed at a high collective pitch angle value (>24 deg). To investigate this particular phenomenon, the transitional criterion previously established at LABM[23] and based on the BL second thickness of energy δ'_3 has been checked. This criterion has been applied for all concerned collective pitch angles and x/c positions. The following equation gives the formulation of this criterion, which is able to detect the BL transition from a laminar state to a turbulent one:

$$\left(Re_{\delta'_3}\right)_t = 0.0135 \cdot \left\{1 + 1.5 \exp\left[-\left(Re_x/3.5 \times 10^4\right)\right]\right\} \cdot Re_x^{0.8} \quad (4)$$

In the present study Reynolds number Re_x is constant for all the chordwise stations located at $r/R = 0.30$ and $Re_{\delta'_3}$ is represented by a straight line in Fig. 10. Figure 10 clearly shows a laminar BL at $x/c = 0.10$ and for $10.22 < \theta_{r/R=0.3} < 24.75$ deg; a turbulent BL at $x/c = 0.54$ and for $10.22 < \theta_{r/R=0.3} < 24.75$ deg; a laminar BL for $x/c = 0.33$, $\theta_{r/R=0.3} = 10.22$ deg and $x/c = 0.33$, $\theta_{r/R=0.3} = 15.38$ deg; and a turbulent BL for $x/c = 0.33$, $\theta_{r/R=0.3} = 24.75$ deg. Such results give clear information concerning the chordwise position of the transition point of the BL. At $\theta_{r/R=0.3} = 10.22$ deg, the BL transition point is located near the midchordwise station, $x/c \approx 0.48$, where as for $\theta = 15.38$ deg this point is shown to move toward the leading edge, $x/c \approx 0.35$. At $\theta = 24.75$ deg, the BL remains laminar only for $x/c = 0.10$ and the transitional point appears to be located near the leading edge, $x/c \approx 0.18$. Such results are good confirmation of the evolution of experimental and theoretical velocity profiles given in Figs. 8 and 9. It can also be concluded that the separation phenomenon has not been observed for the present parametric conditions. This allows concluding that centrifugal effects provide a significant delay of the BL separation in terms of collective pitch angle values.

V_r Component Behavior

The V_r spanwise velocity component is still difficult to analyze inside the BL because of the measurement discrepancies very close to the wall. Nevertheless, suitable accuracy is obtained on V_r in the potential flow and provides useful data to characterize the flow direction at different chordwise stations of the airfoil section. Table 4 gives the centrifugal or centripetal tendency of the flow over the blade section. In Fig. 11, the flow directions corresponding to different $\theta_{r/R=0.3}$ values are indicated by black arrows. Data for Table 4 are deduced from results obtained in Fig. 7b.

The arrows in Table 4 between $x/c = 0.10$ and 0.33, highlight the influence of the separation point of the airfoil incoming flow in the radial direction. Also note that the absolute value of V_r is more important at the midchord station than at $x/c = 0.33$. This explains the fact that the BL remains always attached even at a high collective pitch value, given that the BL results from composition of both V_t and V_r profiles behaviors. The V_t component is indeed exhibiting a strong decrease at a midchord station and at the three collective pitch angle values, which correspond to the increase on the V_r component at the same location.

Conclusions

The present study concerns an experimental BL analysis in the inboard region of a tilt-rotor blade operating in hover. Specific attention has been paid to the evolution of chordwise V_t and spanwise V_r velocity components. Parametric conditions are the following: $r/R = 0.3$; $M_{\text{tip}} = 0.22$; $x/c = 0.10$, 0.33, and 0.54; and $\theta_{r/R=0.3} = 10.22$, 15.38, and 24.75 deg. V_t and V_r velocities evolution have been measured by means of an ELDV method, which allows a complete survey of the BL from 0.3 to 20 mm ($1 \leq \eta \leq 80$) to the blade surface. The complete analysis of BL profiles has pointed out the following results.

At $\theta_{r/R=0.3} = 15.38$ deg and $x/c = 0.54$, chordwise velocity profiles exhibit a turbulent BL behavior ($1/n$ law), whereas for $x/c = 0.10$ and 0.33, the BL appears to be very thin with a likewise laminar velocity profile.

At $\theta_{r/R=0.3} = 24.75$ deg, the chordwise velocity profile relative to $x/c = 0.33$ exhibits an attached turbulent BL. This particular result indicates the occurrence of a significant delay in terms of collective pitch angles on the BL separation due to rotation.

The spanwise velocity component appears to be very useful to specify the centripetal or centrifugal nature of the flow passing over the blade section. However, the characterization of the BL behavior in the spanwise direction remains difficult and will require technical fundamental and theoretical improvements in the near future.

This work has also contributed to extend the validation range of the transition criterion previously established at LABM and based on the second thickness of energy δ_3'. In future works, this transition criterion will continue to be validated in a wider range of parametric conditions of the tilt-rotor (including collective pitch angles, rotational frequencies, x/c position etc.). The present results have also shown that the ELDV method is well adapted to quantify the BL state in rotation and to measure velocity profile near the surface.

Acknowledgments

This research is partly supported by the European Research Office of the US Army under Contract N62558-02-M5609. The authors are particularly thankful to Chee Tung for his fruitful advice and encouragement during the work.

References

[1]Young, L. A., "Tilt-Rotor Aeroacoustic Model (TRAM): A New Rotorcraft Research Facility," *Proceedings of the AHS International Meeting on Advanced Rotorcraft Technology and Disaster Relief*, 1998.

[2]Young, L. A., Booth, E. R., Jr., Yamauchi, G. K., Botha, G., and Dawson, S., "Overview of the Testing of a Small-Scale Proprotor," *Proceedings of the Fifty-Fifth Annual Forum of the American Helicopter Society*, 1999.

[3]Burley, C. L., Marcolini, M. A., Brooks, T. F., Brand, A. G., and Conner, D. A., "Tilt-Rotor Aeroacoustic Code (TRAC) Predictions and Comparison with Measurements," *Proceedings of the Fifty-Second Annual Forum of the American Helicopter Society*, 1996.

[4]Johnson, W., "CAMRAD II, Comprehensive Analytical Model of Rotorcraft Aerodynamics and Dynamics," Johnson Aeronautics, Palo Alto, CA, June 2000.

[5]Johnson, W., "Calculation of the Aerodynamic Behavior of the Tilt-Rotor Aeroacoustic Model (TRAM) in the DNW," *Proceedings of the Fifty-Seventh Annual Forum of the American Helicopter Society*, 2001.

[6]Corrigan, J. J., and Schillings, J. J., "Empirical Model for Stall Delay due to Rotation," *Proceedings of the American Helicopter Society Aeromechanics Specialists Conference*, 1994.

[7]Schmitz, F. H., "Aeroacoustics of Flight Vehicles: Theory and Practice; Vol. 1: Noise Sources," NASA RP-1258, 1991, Chap. 2.

[8]Burley, C. L., Marcolini, M. A., Brooks, T. F., Brand, A. G., and Conner, D. A., "Tilt-Rotor Aeroacoustic Code (TRAC) Predictions and Comparison with Measurements," *Proceedings of the Fifty-Second Annual Forum of the American Helicopter Society*, 1996.

[9]Booth, E. R., Jr., McCluer, M., and Tadghighi, H., "Acoustic Characteristics of a Model Isolated Tilt-Rotor in the DNW," *Proceedings of the Fifty-Fifth Annual Forum of the American Helicopter Society*, 1999.

[10]Yamauchi, G. K., Burley, C. L., Mercker, E., Pengel, K., and Janakiram, R., "Flow Measurements of an Isolated Model Tilt-Rotor," *Proceedings of the Fifty-Fifth Annual Forum of the American Helicopter Society*, 1999.

[11]Matos, C., Reddy, R., and Komerath, N. M., "Rotor Wake/Fixed Wing Interactions with Flap Deflection," *Proceedings of the Fifty-Fifth Annual Forum of the American Helicopter Society*, 1999.

[12]Carr, L. W., "Progress in Analysis and Prediction of Dynamic Stall," *Journal of Aircraft*, Vol. 25, No. 1, 1988, pp. 6–17.

[13]Berton, E., Favier, D., Nsi Mba, M., Maresca, C., and Allain, C., "Embedded LDV Measurement Methods Applied to Unsteady Flow Investigation," *Experiments in Fluids*, Vol. 30, No. 1, 2001, pp. 102–110.

[14]Carr, L. W., Chandrasekhara, M. S., and Brock, N., "Quantitative Study of Unsteady Compressible Flow on an Oscillating Airfoil," *Journal of Aircraft*, Vol. 31, No. 4, 1994, pp. 892–898.

[15]Goody, M. C., and Simpson, R. L., "Surface Pressure Fluctuations Beneath Two- and Three-Dimensional Turbulent Boundary Layers," *AIAA Journal*, Vol. 38, No. 10, 2000, pp. 1822–1831.

[16]Lee, T., Petrakis, G., Mokhtarian, F., and Kafyeke, F., "Boundary-Layer Transition, Separation, and Reattachment on an Oscillating Airfoil," *Journal of Aircraft*, Vol. 37, No. 2, 2001, pp. 360–365.

[17]Bragg, M. B., Heinrich, D. C., and Balow, F. A., "Flow Oscillation over an Airfoil near Stall," *AIAA Journal*, Vol. 34, No. 1, 1996, pp. 199–201.

[18]Rinoie, K., and Takemura, N., "Oscillating Behaviour of Laminar Separation Bubble Formed on an Airfoil near Stall," *Aeronautical Journal*, Vol. 108, No. 1081, 2004, pp. 153–163.

[19]Alam, M., and Sadham, N. D., "Direct Numerical Simulation of Short Laminar Separation Bubbles with Turbulent Reattachment," *Journal of Fluids Mechanics*, Vol. 410, 2000, pp. 1–28.

[20]Mary, I., and Sagaut, P., "Large-Eddy Simulation of Flow Around an Airfoil near Stall," *AIAA Journal*, Vol. 40, No. 6, 2002, pp. 1139–1145.

[21]Johnson, W., "Airloads and Wake Geometry Calculations for an Isolated Tilt-Rotor Model in a Wind Tunnel," *Proceedings of the Twenty-Seventh European Rotorcraft Forum*, 2001.

[22]Favier, D., Maresca, C., Nsi Mba, M., Berton, E., and Agnes, A., "New Type of Embedded Laser Doppler Velocimeter for Measurement of Rotary Wings Boundary Layer," *Review of Scientific Instruments*, Vol. 68, No. 6, 1997, pp. 2447–2455.

[23]Pascazio, M., Autric, J. M., Favier, D., and Maresca, C., "Boundary-Layer Characterization on Moving Walls by an Embedded Laser Velocimetry Technique," *AIAA Journal*, Vol. 35, No. 1, 1997, pp. 207–209; also AIAA Paper 96-0035, Jan. 1996.